FOCUS: INTERDISCIPLINARY BIOLOGICAL MS: RESEARCH ARTICLE

Trapping Radial Electric Field Optimization in Compensated FTICR Cells

Aleksey V. Tolmachev,[1] Errol W. Robinson,[2] Si Wu,[2] Richard D. Smith,[1] Ljiljana Paša-Tolić[2,3]

[1]Biological Sciences Division, Pacific Northwest National Laboratory, Richland, WA USA
[2]Environmental Molecular Sciences Laboratory, Pacific Northwest National Laboratory, Richland, WA USA
[3]EMSL, MSIN: K8-98, Pacific Northwest National Laboratory, P.O. Box 999 Richland, WA 99352, USA

Abstract
Herein, we present the theoretical and experimental study of the recently introduced FTICR cell designs. We developed an approach that determines the electric field inside the cell, based on the measurement of calibration coefficients as a function of post-excitation radius and other conditions. Using the radial electric field divided by radius (E_r/r) as a criterion of the cell harmonization, we compare the compensated cell approach with alternative designs and discuss practical implications of the cell compensation.

Key words: FT-ICR, FTMS, LC-MS, Cell compensation, Dynamic range, Resolving power, Mass accuracy

Introduction

Currently, there is renewed interest in FTICR MS trapping cell design, and the potential for improved MS measurements, as evidenced by several recently reported designs [1–6]. These designs have been based on the previous cell work [1, 2], prior compensated cell designs [3, 4], or relatively new designs in electrode geometry [5, 6]. The compensated FTICR cell provided improved homogeneity of the radial electric field and allowed operation at excitation radii increased up to 70% of the cell radius [7, 8]. This cell design uses the open cylindrical geometry [9–11] complemented with two pairs of additional shim electrodes, seven cylindrical segments total (Supplemental Figure 1). This cell design is further referred to as OC-7S cell (open cylindrical seven segment cell). Experimental studies confirmed that the mass measurement accuracy (MMA) has improved both in model peptide mixture measurements using internal calibration, and in LC MS complex peptide mixture measurements using an external mass calibration. An alternative approach to cell compensation, recently introduced by the Nikolaev group, segments the cell electrodes using leaf-shaped inserts [5]. With such diverse perspectives on cell design, this work aims to explain motivations, design rationale, and experimental evaluation strategies for the OC-7S cell design and compare this design to alternative FTICR cell designs using evaluation approaches described below.

Theory

A variety of applications exist and are planned for FTICR MS at PNNL, including top-down proteomics, MS imaging, analysis of complex biological systems such as microbial communities, etc., all of which depend critically on MMA, dynamic range, and sensitivity.

Previous MMA studies revealed deviations from an ideal calibration law, depending on excitation power, ion population, etc. [12–16]. Ideally, if there is no electric field, the cyclotron frequency of an analyte ion, ω_c, is readily

Correspondence to: Ljiljana Paša-Tolić; *e-mail:* Ljiljana.pasatolic@pnl.gov

determined, as shown in Equation (1), where m/z is the mass to charge ratio of the analyte ion and B_z is the magnetic field inside of the ion trapping cell:

$$\omega_c = \frac{e}{m_u\, m/z} B_z \qquad (1)$$

This and subsequent equations are using SI units; elementary charge e equals $1.60217733 \times 10^{-19}$ C and unit mass m_u is $1.66053873 \times 10^{-27}$ kg. Assuming a uniform magnetic field, the cyclotron frequency of the ion is constant through the whole cell volume. But, an electric field is needed to confine the ions inside the trapping cell during excitation and detection for useful measurements to be obtained. As a result of this ion trapping, or axial confinement, a radial electric field E_r is created. The spatially variable radial electric field produces frequency variations, or magnetron frequency shifts $\Delta\omega$, in the observed effective ion cyclotron frequency:

$$\Delta\omega = \frac{E_r}{r} \cdot \frac{1}{B_z} \qquad (2)$$

This equation can be derived based on the effective ion cyclotron frequency relationship for the quadrupolar trapping potential [17–19], where E_r/r is constant throughout the volume; considering small variations of this quantity, one can use Equation (2) as an approximation, assuming "local", or ion motion-averaged values for E_r/r [7]. We note that the magnetic field inhomogeneity creates an additional source of frequency variations, which can be treated separately; here we are focusing on the electric field effect. The open cylindrical ion trapping cell geometry [9–11] has a typical profile of the DC trapping potential, Supplementary Figure 2a, which produces a characteristic profile of the radial field that has both a negative and a positive spike at the edges of the central cylinder. In typical measurements, e. g. online LC-FTICR MS, the ions successfully injected into the cell have ~1 eV (order of magnitude) variations in axial kinetic energy. Using Equation (2) shows that the radial field variations characteristic for the noncompensated cell (Supplementary Figure 2a) can produce over 10 ppm variation in the effective cyclotron frequency, which then results in mass measurement errors of the same magnitude [7]. Equation (2) shows that the radial field variations characteristic for the noncompensated cell (Supplementary Figure 2a) can produce over 10 ppm variation is the effective cyclotron frequency, which then results in mass measurements errors of the same magnitude [7]. This demonstrates the relative potential improvement using compensation cell designs, but does not mean that all open cylindrical cells will perform with a 10 ppm MMA. Many factors influence MMA, including magnetic field strength and homogeneity, ion population, and cell geometry. Here we focus on the impact of the electric field on cell performance. Increased mass

errors due to electric field take place when the excited ion motion occupies a cell volume extending to the areas of increased variations of E_r/r quantity. The ppm range for mass accuracy is obtained with the noncompensated cell using reduced ion excitation radii [7]; reduction of the axial spread of the ion motion also helps.

The goal of maximizing MMA requires the cell optimization procedure to minimize the frequency shift term corresponding to the cell volume occupied by ions during detection. The approach also minimizes frequency shifts due to ion–ion interactions, by enabling the use of increased excitation radii [7]. The goal can be achieved by creating a potential distribution close to the quadrupolar potential [3, 4, 20]:

$$V(r,z) = V_0 \left(\frac{z^2}{a^2} - \frac{r^2}{2a^2} \right) + C \qquad (3)$$

Here, the cylindrical coordinate system (r, z) is assumed with radius $r = (x^2 + y^2)^{0.5}$, axial coordinate z, measure of the trap size a, and constant C. Such an ideal quadrupolar potential can be realized in a Penning trap that has electrodes shaped according to equipotential surfaces of the ideal potential distribution (Equation 3). The radial electric field divided by radius can be obtained by taking the second derivative of potential as defined in Equation (3):

$$E_r/r = V_0/a^2 \qquad (4)$$

The right-hand side is independent of coordinates r, z, which implies that the magnetron frequency shift (Equation 2) is constant throughout the volume, an ideal scenario for minimizing the variation in the observed cyclotron frequency. The cyclotron frequency is shifted due to the trapping potential and utilizing a quadrupolar trapping potential does not minimize the absolute magnitude of this frequency shift. The frequency shift term is constant within the volume of the ion trapping cell resulting in zero deviations in the observed cyclotron frequency. This configuration fulfills assumptions underlying the FTICR calibration functions [17–19], and thus approaches the maximum precision for FTICR mass measurements, achievable in the limit of low ion-ion interactions and the uniform magnetic field.

Experimentally, the approach of creating a potential distribution described by Equation (3) was evaluated based on measurements of calibration coefficients as a function of post-excitation radius. The radial electric field distribution of the OC-7S cell was also compared with that of the ring [3, 4] and leaf [5] cells, as described below.

Experimental

The OC-7S cell design and initial evaluation in a modified Bruker 12 T FTICR have been previously described [7]. The cell design features an open cylindrical geometry modified

to include two pairs of compensated trapping potential rings, Supplemental Figure 1. Each of the seven cylindrical segments was split into four sectors, two for detection and two for excitation, with capacitive coupling applied to the excitation sectors of all segments. Free induction decay (FID) was acquired at the two detection sectors of the central segment. An unmodified open cylindrical cell was approximated by changing the DC potential values of the compensation segments. While these values were known to be nonoptimal, measurement and simulation results using these DC potentials were useful experimental controls. Specifically, the compensation electrodes closest to the central segment were set to 0 V and those closest to the trapping segments to the trapping potential of the cell (Supplemental Figure 2a). Typically, the compensation segments potentials would be set to the optimized values that minimize deviations from the quadrupolar potential distribution (Supplemental Figure 2b). Here, we switched between the two cell voltage configurations to demonstrate the effectiveness of the compensation electrodes and "open cell" refers to the voltage configuration closest to that of a typical cylindrical cell (Supplemental Figure 2a) while "compensated cell" refers to the voltage configuration closest to the ideal potential distribution (Supplemental Figure 2b).

Mass spectra with up to 12 calibrant ions were acquired on a modified Bruker 12 Tesla FTICR mass spectrometer [7, 8], using electrospray ionization of an aqueous solution of a peptide mixture. The solution consisted of 0.1% acetic acid, 0.025% trifluoroacetic acid, and 0.5 μg/ mL of each of the following peptides acquired from Sigma-Aldrich (St. Louis, MO, USA) used as received: renin inhibitor, bradykinin, neurotensin, angiotensin, Substance P, fibrinopeptide A, and G endorphine.

Mass spectra of this solution were previously acquired over a range of excitation powers, external accumulation times, and cell trapping voltages in automated fashion using Xmass (Bruker Daltonics, Billerica, MA, USA) scripts [7, 8]. We have reanalyzed these results using a new procedure to evaluate the experimental cell performance. Briefly, mass spectra were acquired for excitation attenuation ranging from 0 to 20 dB, external accumulation times were 0.05, 0.1 and 0.2 s and cell trapping voltages were 1 to 4 V. Results for trapping voltage 4 V are reported here. Experimental conditions follow the cell characterization experiments [7], hence the choice of ion excitation range (dB) and cell trapping voltage of 4 V. External accumulation was performed in the standard Bruker hexapole with a short pulse of gas to increase trapping efficiency. Collections of spectra were processed using in-house developed software to characterize instrument performance. Each transient was zero-filled twice, Fourier-transformed, and converted to the m/z domain. Zero-filling twice was found useful, because each zero-filling step reduces (two times) the frequency step of the Fast Fourier Transform procedure; the four times smaller frequency step has allowed us to reproducibly obtain mass measurement accuracy of the order of 0.01 ppm, both

for the compensated and for the noncompensated cell [7]. The MMA of the internal calibration was calculated as RMS of relative mass errors from internal calibration of peptide, as reported in [7]. The internal calibration produced calibration coefficients, which provided a measure of the electric field distribution.

The ring and leaf cell designs were compared with the OC-7S compensated cell design using an approach similar to that applied to the OC-7S cell and described previously [7]. Considered here are results of the 3D potential modeling, which we have found useful for prediction of cell performance, as validated by the experimental data obtained for the OS-7S cell.

Results and Discussion

Cell Compensation Design Approach

As previously mentioned (see Equation 2), the variation in the observed cyclotron frequency of an ion directly relates to the radial electric field, E_r. Herein, we have used the Laplace equation to solve for the electric potential inside the volume of the ion trapping cell. This analysis was greatly simplified, so that constraints on key cell geometry relationships can be determined by taking advantage of three key properties of Laplace equation:

(1) Linear superposition principle: the potential distribution is expressed as a sum of distributions produced by each electrode, weighted according to the voltage applied to that electrode.
(2) The potential acquires ideal-like distribution when boundary condition imperfections are small, or near the axis or plane of symmetry, far from the boundary.
(3) The scale rule: the characteristic size of the region where the added potential is created is defined by the size of the added electrode. In other words, electrode surfaces have the most impact in a specific trapping cell volume, which can be roughly estimated as comparable to the size of the electrode surface.

These three properties of Laplace equations guided the establishment of constrained ranges of cell geometries. For example, if the width of cell compensation electrodes, d, was narrow respective to radius of the ion trapping cell, R_c (i.e., $d \ll R_c$) then a relatively high voltage was required for the narrow compensation electrode to have a significant impact on the electric potential in the center of the field. These high compensation voltages proved to be disruptive to the naturally smooth behavior of the ideal harmonic potential distribution. This could perhaps be overcome by the use of many compensation rings, but this would also increase the mechanical and electrical complexity of the FTICR cell design.

On the other hand if the width of the compensation electrode is larger than the cell radius, $d >\sim R_c$, then

boundary condition perturbations, or electrode edge effects, penetrated inside the cell, which ultimately resulted in larger radial electric field variations and introduced a variations of E_r/r as a function of distance from the center axis of the cell. This effect was observed as a reduction in MMA at higher excitation powers as ions were excited to regions of the cell further from the center of the cell, closer to the electrode surfaces, contradicting the goal of a smooth behavior up to high radial positions, $>\sim 0.5\ R_c$. These thought exercises, confirmed by potential calculations of various cell geometries, defined useful compensation segments widths to be a relatively narrow range of values, approximately half the cell radius, $d\sim 0.5\ R_c$. Consequently, the OC-7S cell geometry utilizes a pair of compensation segments on each side of the detection segment with compensation segments widths, d, equal to 0.4 R_c.

Similar considerations regarding the width of the central segment with opposing pairs of excitation and detection electrodes suggest the width of this segment equal to the cell radius R_c. Considering the plane of symmetry crossing the central segment, we effectively obtain three steps of gradually changing potential at each side; the steps having width 0.5, 0.4, and 0.4 (units R_c). This approach allowed us to use a smooth profile of voltages: 1, 0.3167, 0.1333, 0, 0.1333, 0.3167, 1 (in relative units) to achieve a potential distribution that closely approximates the desired harmonic potential field at the cell axis. The corresponding axial potential profile is shown in the compensated cell diagram, Supplemental Figure 2b. This electrode configuration was the final result of a series of iterative cell designs followed by potential calculations to evaluate the variation in the radial electric field divided by radius.

The resulting compensated electrode configuration succeeded in reducing variation in the cyclotron shift for a significant volume of the trapping cell. This proved to have profound significance in cell performance [7, 8]. Briefly, minimizing the variation of radial electric field in the whole cell volume enables the use of larger cyclotron excitation radii, which in turn improves sensitivity and dynamic range. The larger cyclotron excitation radii also reduced columbic interaction effects, which could further be reduced by the use of variable, non uniform, or spread excitation, as shown by Marshall and coworkers [2]. Because the considered approach to optimization of the cell electrode geometries is based on the radial electric field per radius, E_r/r, we have conducted an experimental study to characterize this property for compensated and open cylindrical cell geometries below.

Experimental Study of the Radial Electric Field

We present here an approach that directly measures the radial electric field and perform these calculations on datasets acquired in ref [7]. The approach is based on a property of the FTICR calibration function that allows one to express the electric field related frequency shifts via the calibration coefficient values. Consider first the classical

FTICR calibration function first proposed by Ledford et al. [18]:

$$m/z = \frac{A_L}{f} + \frac{B_L}{f^2} \qquad (5)$$

Two calibration coefficients A_L, B_L can be expressed via magnetic and radial electric field intensities [18, 19]:

$$A_L = \frac{eB_z}{2\pi m_u} \qquad (6)$$

$$B_L = \frac{e}{4\pi^2 m_u} \cdot \frac{E_r}{r} \qquad (7)$$

Here e is electron charge and m_u is unit mass constant, $m_u = 1.660539 \times 10^{-27}$kg. The effective ion cyclotron frequency f can be expressed as a sum of the unperturbed cyclotron frequency, Equation 1, and a frequency shift Δf_E, produced by electric fields:

$$f = \frac{\omega_c}{2\pi} + \Delta f_E \qquad (8)$$

$$\Delta f_E = \frac{B_L}{A_L} = \frac{1}{2\pi B_z} \cdot \frac{E_r}{r} \qquad (9)$$

It should be noted that experimentally observed frequency shifts are negative, so that the observed cyclotron frequency f is smaller than the unperturbed cyclotron frequency $\omega_c/2\pi$; the calibration coefficient B_L is generally negative.

Equations 5, 6, 7, 8, 9 are often considered in a framework of the idealized quadrupolar electric potential distribution, Equation 3. In this case the radial field expression Equation 4 can be substituted in Equation 9, resulting in the frequency shift proportional to the cell trapping potential V_0, and independent of the post-excitation radius r. However, Equation 9 can be also used as an approximation for any practical case where the calibration function Equation 5 is applied. In this case, the electric field E_r can be considered as a sum of the DC trapping field, space charge fields and other electric fields that influence the ion cyclotron frequency.

Similar relationships can be obtained for another FTICR calibration function, originally proposed by Francl et al. [17]:

$$m/z = \frac{A_F}{f + B_F} \qquad (10)$$

Using power series expansion, as demonstrated previously [19], it can be shown that the two sets of calibration coefficients are related as follows:

$$A_F = A_L \qquad (11)$$

$$B_F = -B_L/A_L \qquad (12)$$

The frequency shift due to electric field is equal to the Francl's B-coefficient, with reversed sign:

$$\Delta f_E = -B_F \tag{13}$$

We conclude that the calibration coefficient values can be used as a measure of the electric field related frequency shifts. It is convenient to use the Francl's form of the calibration function for characterization of frequency shifts, using the simple Equation 13. Because of extremely high accuracy typical for FTICR mass calibration, this method is very sensitive to small variations of the radial electric field. The coefficient A in either of the two calibration functions gives a measure of the magnetic field, Equations 6 and 11. The A values obtained for a range of excitation power and axial kinetic energy can be used to evaluate the magnetic field spatial distribution, an approach complimentary to using the NMR probe. The initial cell study reported total ion current (TIC), signal life-time and MMA characteristics obtained using ESI of a mixture of 9 peptides [7]. Here, each spectrum was calibrated based on up to 12 calibrant ions corresponding to single and doubly charged peptide ions. The post-excitation radius was calculated as described previously [7]. Figure 1a and b show the calibration coefficient B_F obtained in these measurements. Corresponding frequency shifts Δf_E due to electric field vary in the range 20 to 60 Hz. Compared with the cyclotron frequency of 184 KHz (B_z 12 Tesla, m/z 1000), the frequency shift is 100 to 300 ppm. This "global" frequency shift should not be confused with m/z-specific, "local" frequency shifts that constitute mass measurement errors and are much smaller, thanks to the calibration function accounting for a major part of the electric field related frequency shift. Recall that we can effectively calibrate for a constant frequency shift and that it was variation in the frequency shift that we sought to minimize during the modeling of various cell geometries. The frequency shifts in Figure 1a and b increase at low post-excitation radii and higher ion populations (i.e., longer external accumulation times), which can be attributed to Columbic interactions also termed space charge effects. In this region, the classical calibration functions are not accurate, and various corrections can be used [13, 15, 18, 21–23]. These results also demonstrate the benefit of using increased ion excitation to achieve higher post-excitation cyclotron radii to reduce columbic interactions and improve MMA, provided the variations of E_r/r remain sufficiently small.

The B_F coefficient profiles obtained for the noncompensated cell, Figure 1a, markedly differ from ones obtained for the compensated cell, Figure 1b. To understand this behavior, we have compared the experimental data with B_F coefficient values calculated using Equation 9. The radial electric field was calculated based on potential simulations done for the both cell configurations, as described previously [7]. Red curves in Figure 1a and b, show B_F coefficients
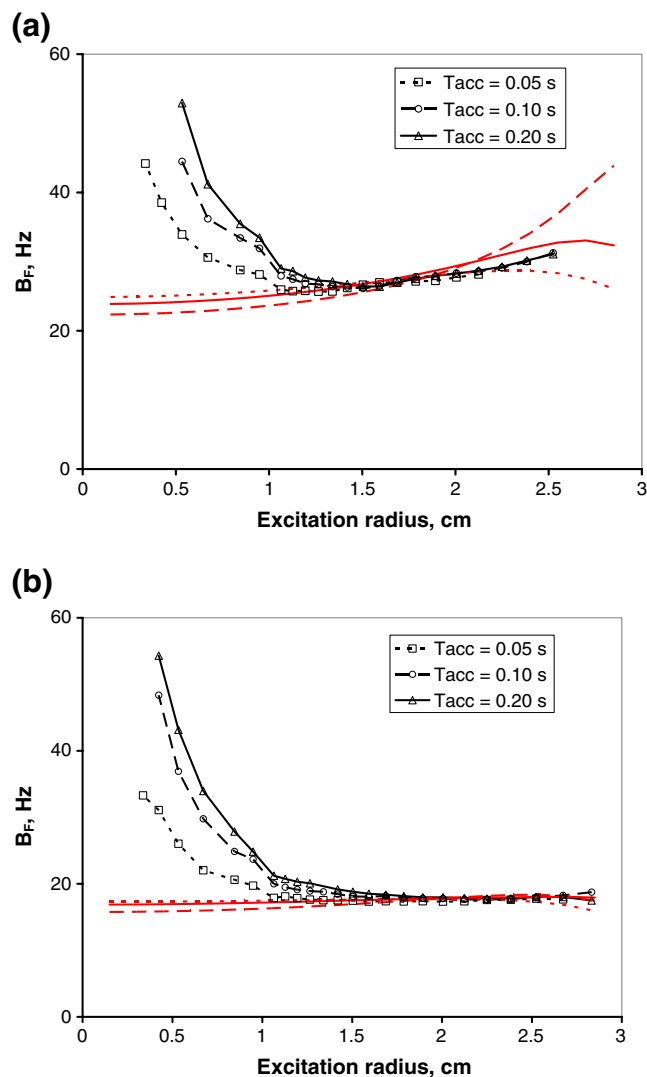
Figure 1. Electric field related frequency shifts, measured as the Francl's calibration coefficient B_F: (**a**) noncompensated cell, (**b**) compensated cell. A mixture of nine peptides was used to obtain the internal calibration; spectra were obtained for a range of excitation powers and three different levels of ion population, controlled via the external accumulation time Tacc=0.05 s (*squares*), 0.10 s (*circles*), and 0.20 s (*triangles*). Red curves: B_F coefficient calculated using the radial electric field obtained from potential calculations for the two corresponding configurations, for three values of the axial kinetic energy of ions: K_z=0.5 eV (*dotted*), 0.8 eV (*solid*), and 1.2 eV (*dashed*)

calculated assuming three different ion kinetic energies: K_z= 0.5 eV (dotted), 0.8 eV (solid), and 1.2 eV (dashed). These energies corresponded to upper boundaries of z-oscillations Z_{max}=2, 2.4, and 3 cm for the compensated cell and 1.8, 2.1, and 2.4 cm for the noncompensated cell. These results were obtained with the radial electric field, $E_r(r, z,)$ averaged in the range 0 to Z_{max}.

The calculated frequency shifts closely approach experimental results in the range of excitation radii where the space charge contribution is not significant, >~1.5 cm, or 50% of the cell inner radius, thus confirming that the DC voltages applied to the seven cylindrical segments produce the desired effect on the ion motion. The noncompensated cell B_F coefficient profiles vary noticeably with radius and z-axis range, while the compensated cell shows much smaller radius and z-axis dependent variations. The mass calibration accuracy improvement due to compensation reported previously [7], can be explained in part by the improved spatial uniformity of the B-coefficient (due to reduced variation in radial electric field). Another important factor is the compensated cell ability to use higher excitation radii and thus reduce space charge effects. B_F coefficient uniformity in the axial direction makes mass calibration less sensitive to the ion kinetic energy. This is particularly important for LC MS measurements, where changing ion populations can be translated to variations in the kinetic energy of ions ejected from the external accumulation multipole [20, 24, 25].

Recent compensated cell publications initiated the discussion whether theoretically obtained potentials should be applied directly or optimum values must be experimentally determined [1–4]. Figure 1 demonstrates that using the theoretically calculated compensation voltages does in fact deliver the desired outcome in terms of the ion frequency profiles, suggesting that the use of the theoretical compensated potentials is at least a valid starting point. Further adjustments can be done as reported by Marshall and coworkers [1, 2] if there are reasons to believe that conditions differ from conditions used for the cell optimization (e.g., in the case of increased spreads in the axial kinetic energy, or in an attempt to compensate frequency shifts due to a magnetic field inhomogeneity). However, a more consistent approach in such cases would be to understand the fundamental cause of the deviations from the ideal and use an adequate cell compensation approach. Particular attention should be given to E_r/r profiles at increased excitation radii not only due to the advantages of reduced columbic interactions and increased sensitivity, but also due to the fact that the effectiveness of cell compensation strategies is more apparent at larger excitation radii (>0.5 cell radii) as the ions approach the electrode surfaces.

Ring Cell Design Approach

It is interesting to explore how a different set of optimization criteria can result in a quite different cell design. A recent study [3] stated that the harmonic, or quadrupolar, potential would result in optimal cell performance. However to achieve this goal, the authors utilized a different FTICR cell design strategy based upon minimizing electric field variation in the center of the cell. The resulting ring cell design features three relatively narrow compensation rings with an electrode width of 0.1 times the cell radius R_c. We can anticipate from previous discussion that relatively large

compensation voltages will be required to significantly affect the radial electric field near cell center. This will result in significant deviations in the variation of electric field, particularly at larger excited cyclotron radii as the ions approach closer to the compensation electrodes. Figures 2 and 3 present an analysis of the ring cell using the methodology of evaluating the variation in radial electric field. Figure 2a and b show the calculated potential distributions for the ring cell and for the open cylindrical cell without compensation, respectively. The ring cell design results in pronounced waves of the DC potential at radial positions greater than ~0.7 the cell radius. At the high radial positions the potential distribution is not improved, but in fact is deteriorated compared with the uncompensated open cylindrical cell. The ring cell operation at increased ion excitation radii should be sensitive to the range of z-oscillations, which in turn is a function of the ion axial
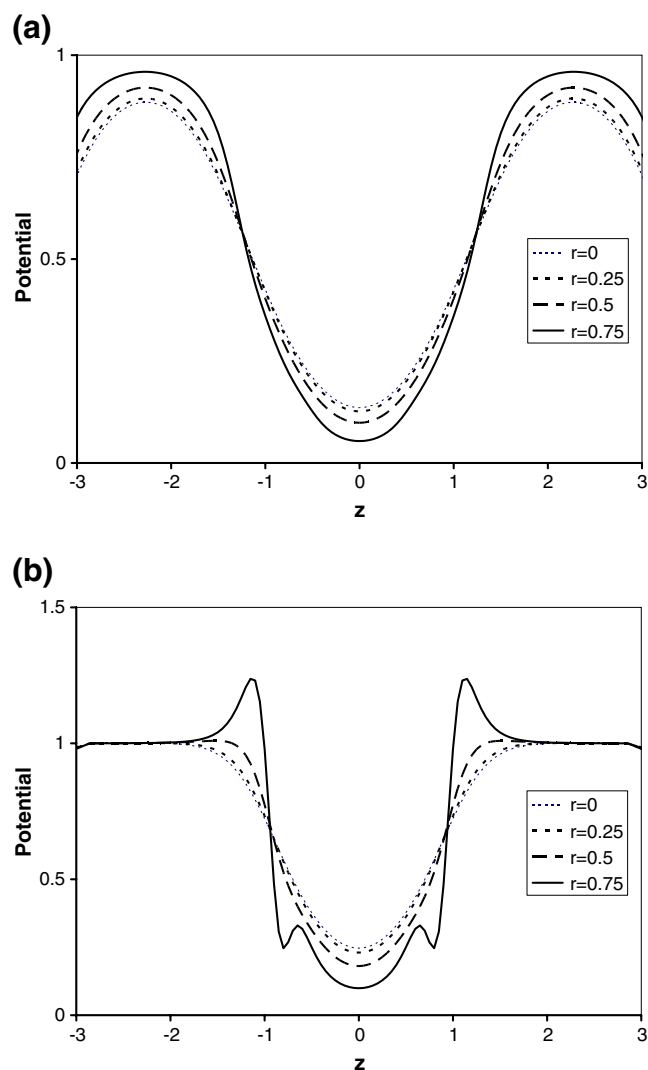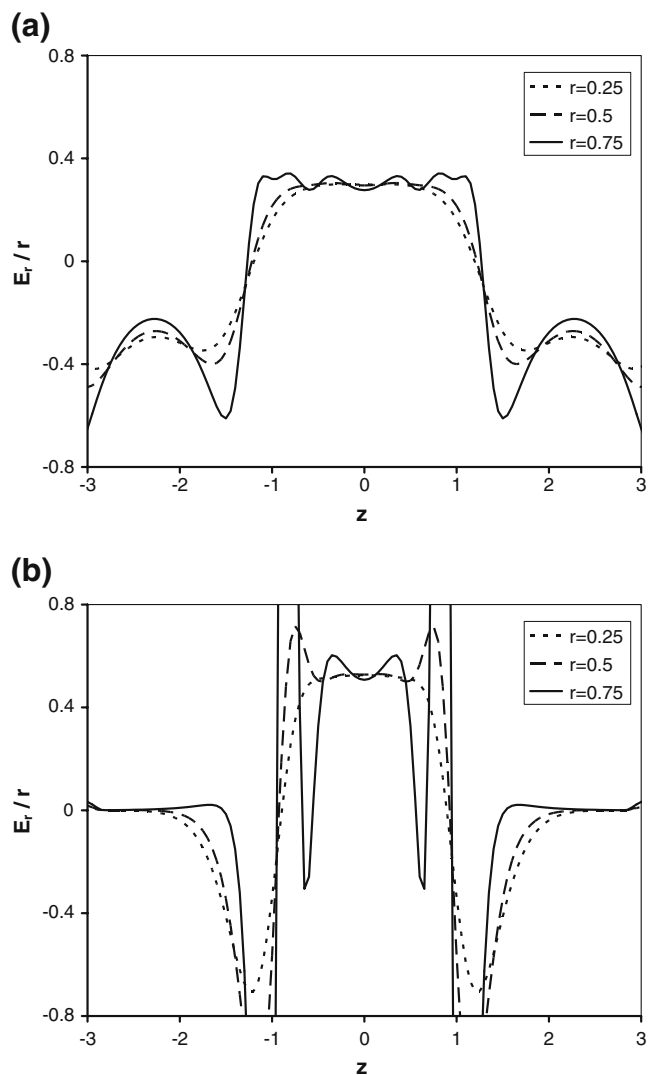

(a)

(b)

Figure 2. Potential distribution calculated for (**a**) the noncompensated open cylindrical cell and (**b**) ring cell, a configuration using three pairs of the compensation segments [3, 4]

(a)

(b)

Figure 3. Radial electric field divided by radius (E_r/r) calculated for (**a**) OC-7S cell and (**b**) ring cell, an approach using three pairs of the compensation segments [3, 4]

kinetic energy distribution, leading to non-optimal performance in LC MS mode of operation.

Let's consider the spatial distribution of the radial electric field per radius, the quantity that defines the magnetron frequency. As seen in Figure 3a and b, the E_r/r profiles of the ring cell in fact achieve the sought improvement in a small region around the point chosen for optimization, r=0.4 R_c, within axial range $<\sim$ 0.5 R_c. The field noticeably deviates from ideal beyond this region and especially at larger cell radius. The large fluctuations in radial electric field for trapping potential of 1 V are produced due to the relatively high compensation voltages having changing polarity: +9.608, −7.608, +9.608 V. To summarize, the potential calculations for the ring cell indicate that this design produces a small region of improved radial field, but also creates significant electric field variations outside of the optimization region. This result can be intuitively interpreted in terms of the

Laplace equation tendency to create smooth potential distributions, when small perturbations are introduced.

Leaf Cell Design Approach

Yet another approach to cell compensation was introduced recently [5]. This approach uses a clever, leaf shaped sectioning of the cylindrical cell geometry. The excitation and detection sections were in the form of leafs, complemented by "inverse leaf" segments onto which the trapping potential was applied. The assembly is cut into four sectors, two for excitation and two for detection. The potential harmonization was achieved by choosing the leaf profile that delivers close to harmonic behavior at the cell axis. While several different leaf geometries and differing numbers of leaves could be used in such leaf cells, we have chosen a quadratic leaf shape, with the cell aspect ratio of two (Figure 4), and analyzed the leaf cell designs with eight and 16 leaves by means of 3D potential calculations. The eighth order cell produced increased off-axis deviations of potential in accordance with the scale rule described above. A significant improvement in the variation of electric field per radius was observed with the 16th order cell (not shown). Figure 5a illustrates the lack of cylindrical symmetry inherent in cells with sectioning parallel rather than perpendicular to the magnetic field. The impact of this variation on the attainable MMA is still under investigation. Figure 5b shows axial electric field profiles for the eighth order leaf cell with the radial electric field per radius at two polar angles, corresponding to a minimum and a maximum of the angular dependence. Under the framework of the approach, we can conclude that the low excitation power regime can be of immediate use with the leaf cell because the angular variations are decreased in the par-axial region of the cell, where a nearly symmetric harmonized potential distribution is created. Compared with the OC-7S cell, this cell provides an elongated volume of the harmonized potential. The low excitation power operation can be of particular interest for large biomolecular ion studies, such as
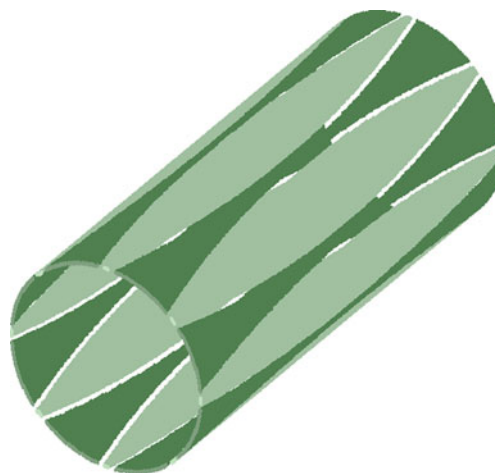
Figure 4. Leaf cell of the eighth order

(a)

(b)
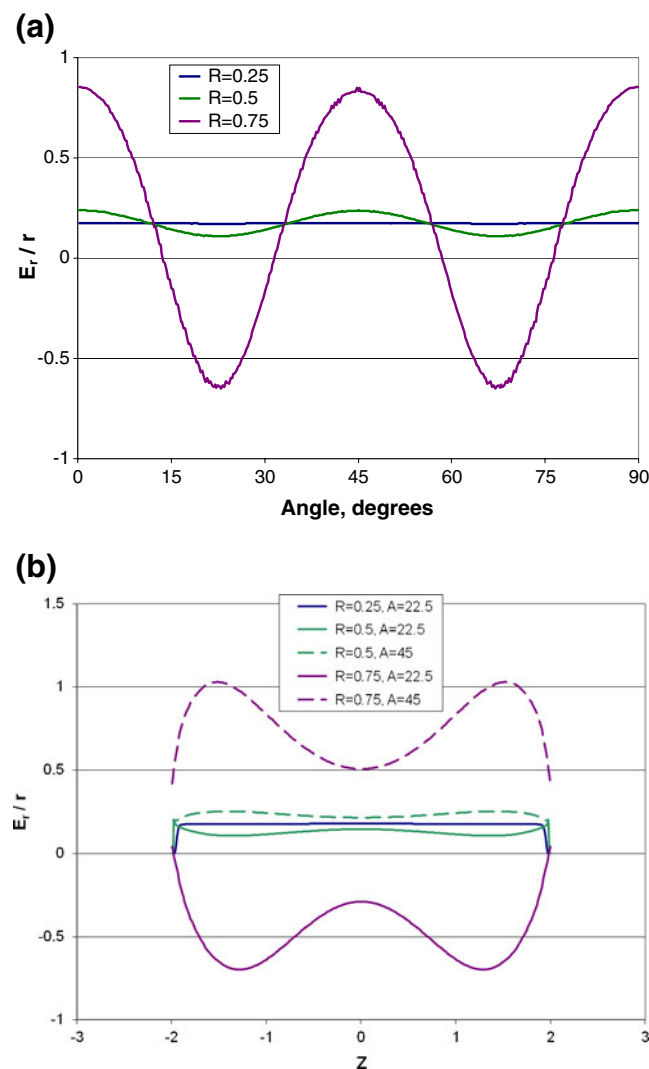
Figure 5. E_r/r profiles for the eighth order leaf cell [5]. (**a**) Angular dependence at $z = 1$ R_c. (**b**) Axial profiles for three radial positions, 0.25, 0.5 and 0.75 R_c, for two polar angles, corresponding to a minimum and a maximum of the angular dependence

encountered in top-down proteomics [8]. We expect, however, that the high excitation power mode that was found useful with the OC-7S can be more difficult to realize with the leaf cell, due to the pronounced angular sways of the radial field.

Conclusions

We developed an approach to experimentally measure the electric field inside of an FTICR ion trapping cell based on the determination of calibration coefficients as a function of post-excitation radius. We have also incorporated other relevant cell parameters such as different ion populations, cell trapping voltages, etc. The harmonic compensated cell, OC-7S configuration, has shown a marked improvement in uniformity of the radial electric field relative to an open

cylindrical cell with no compensation, in close agreement with the theoretical cell design calculations. These measurements validate the use of the radial electric field divided by radius (E_r/r) as a criterion of the cell harmonization. The homogeneous electric field distribution translates into MMA improvement and makes FTICR operation less sensitive to variations of ion kinetic energy (e.g., better LC MS performance). Signal intensity, dynamic range, and sensitivity are also improved mainly due to the improved stability of the E_r/r profile thus enabling the use of increased ion excitation radii.

The two orthogonally-shimmed cells, the OC-7S cell and ring cell, differ in design and in experimental performance. OC-7S cell design aims at electric field correction over a large portion of the cell volume, while the alternative approach, ring cell, focuses at one point in the cell plane of symmetry, and delivers a higher order correction for formally defined ion trajectory at the expense of increased variation in electric field outside of the strictly optimized cell region.

The third approach, longitudinally shimmed leaf cell, aims at creating a trapping potential distribution close to the quadrupolar one, Equation 3, similar to the OC-7S cell. However, the quadrupolar potential is approached only after averaging the angular dependence, under an assumption of perfectly circular and centered ion trajectory. The ion motion in FTICR cell generally consists of a combination of the cyclotron and magnetron motion and is not circular, and the process of ion excitation is not symmetric. The potential calculations reported here have shown intense angular variations of the radial electric field, the behavior unique for FTICR and not studied previously, either theoretically or experimentally. We note that the angular variations are decreased in the par-axial region of the cell, where a nearly symmetric harmonized potential distribution is created. Compared with the OC-7S cell, leaf cell provides a more elongated volume of the harmonized potential, however, for radial positions closer to the center of the cell. The low excitation power operation can be of particular interest for large bio-molecular ion studies, such as encountered in top-down MS [8]. We expect, however, that the high excitation power mode that was found useful with the OC-7S cell will be more difficult to realize with the leaf cell due to the pronounced angular sways of the radial field.

Acknowledgments

References

1. Marshall, A.G.: Overview: Recent Advances in Fourier Transform Ion Cyclotron Resonance Mass Spectrometry, WOBpm, (217) *Proceedings of the 58th ASMS Conference on Mass Spectrometry and Allied Topics*; Salt Lake City, UT, May 23–27, 2010

2. Kaiser, N.K., Savory, J.J., Mckenna, A.M., Hendrickson, C.L., Marshall, A.G.: Tailored Ion Spatial Distribution in FT-ICR MS for Improved Analysis of Complex Mixtures, WOBpm, (221) *Proceedings of the 58th ASMS Conference on Mass Spectrometry and Allied Topics*; Salt Lake City, UT, May 23–27, 2010

3. Brustkern, A.M., Rempel, D.L., Gross, M.L.: An electrically compensated trap designed to eighth order for FT-ICR mass spectrometry. *J. Am. Soc. Mass Spectrom.* **19**, 1281–1285 (2008)

4. Brustkern, A.M., Rempel, D.L., Gross, M.L.: A tuning method for electrically compensated ion cyclotron resonance mass spectrometer traps. *J. Am. Soc. Mass Spectrom.* **21**, 451–454 (2010)

5. Boldin, I.A., Nikolaev, E.N.: Fourier transform ion cyclotron resonance cell with dynamic harmonization of the electric field in the whole volume by shaping of the excitation and detection electrode assembly. *Rapid Commun. Mass Spectrom.* **25**, 122–126 (2011)

6. Misharin, A.S., Zubarev, R.A., Doroshenko, V.M.: Fourier transform ion cyclotron resonance mass spectrometer with coaxial multi-electrode cell ('O-trap'): first experimental demonstration. *Rapid Commun. Mass Spectrom.* **24**, 1931–1940 (2010)

7. Tolmachev, A.V., Robinson, E.W., Wu, S., Kang, H., Lourette, N.M., Paša-Tolić, L., Smith, R.D.: Trapped-ion cell with improved DC potential harmonicity for FT-ICR MS. *J. Am. Soc. Mass Spectrom.* **19**, 586–597 (2008)

8. Tolmachev, A.V., Robinson, E.W., Wu, S., Paša-Tolić, L., Smith, R.D.: FT-ICR MS optimization for the analysis of intact proteins. *Int. J. Mass Spectrom.* **287**, 32–38 (2009)

9. Beu, S.C., Laude, D.A.: Open trapped ion cell geometries for fourier-transform ion-cyclotron resonance mass-spectrometry. *Int. J. Mass Spectrom. Ion Procesess* **112**, 215–230 (1992)

10. Beu, S.C., Laude, D.A.: Elimination of axial ejection during excitation with a capacitively coupled open trapped-ion cell for fourier-transform ion-cyclotron resonance mass-spectrometry. *Anal. Chem.* **64**, 177–180 (1992)

11. Gabrielse, G., Mackintosh, F.C.: Cylindrical penning traps with orthogonalized anharmonicity compensation. *Int. J. Mass Spectrom. Ion Processes* **57**, 1–17 (1984)

12. Easterling, M.L., Mize, T.H., Amster, I.J.: Routine part-per-million mass accuracy for high-mass ions: space-charge effects in MALDI FT-ICR. *Anal. Chem.* **71**, 624–632 (1999)

13. Frahm, J.L., Velez, C.M.C., Muddiman, D.C.: Understanding the influence of post-excite radius and axial confinement on quantitative proteomic measurements using fourier transform ion cyclotron resonance mass spectrometry. *Rapid Commin. Mass Spectrom.* **21**, 1196–1204 (2007)

14. Hawkridge, A.M., Nepomuceno, A.I., Lovik, S.L., Mason, C.J., Muddiman, D.C.: Effect of post-excitation radius on ion abundance, mass measurement accuracy, and isotopic distributions in fourier transform ion cyclotron resonance mass spectrometry. *Rapid Commun. Mass Spectrom.* **19**, 915–918 (2005)

15. Masselon, C., Tolmachev, A.V., Anderson, G.A., Harkewicz, R., Smith, R.D.: Mass measurement errors caused by "Local" frequency perturbations in FTICR mass spectrometry. *J. Am. Soc. Mass Spectrom.* **13**, 99–106 (2002)

16. Taylor, P.K., Amster, I.J.: Space charge effects on mass accuracy for multiply charged ions in ESI-FTICR. *Int. J. Mass Spectrom.* **222**, 351–361 (2003)

17. Francl, T.J., Sherman, M.G., Hunter, R.L., Locke, M.J., Bowers, W.D., McIver, R.T.: Experimental-determination of the effects of space-charge on ion-cyclotron resonance frequencies. *Int. J. Mass Spectrom. Ion Processes* **54**, 189–199 (1983)

18. Ledford, E.B., Rempel, D.L., Gross, M.L.: Space-charge effects in fourier-transform mass-spectrometry—mass calibration. *Anal. Chem.* **56**, 2744–2748 (1984)

19. Shi, S.D.H., Drader, J.J., Freitas, M.A., Hendrickson, C.L., Marshall, A.G.: Comparison and interconversion of the two most common frequency-to-mass calibration functions for fourier transform ion cyclotron resonance mass spectrometry. *Int. J. Mass Spectrom.* **195**, 591–598 (2000)

20. Tolmachev, A.V., Udseth, H.R., Smith, R.D.: Charge capacity limitations of radio frequency ion guides in their use for improved ion accumulation and trapping in mass spectrometry. *Anal. Chem.* **72**, 970–978 (2000)

21. Wong, R.L., Amster, I.J.: Sub part-per-million mass accuracy by using stepwise-external calibration in fourier transform ion cyclotron resonance nass spectrometry. *J. Am. Soc. Mass Spectrom.* **17**, 1681–1691 (2006)

22. Zhang, L.K., Rempel, D., Pramanik, B.N., Gross, M.L.: Accurate mass measurements by fourier transform mass spectrometry. *Mass Spectrom. Rev.* **24**, 286–309 (2005)

23. Williams, D.K., Muddiman, D.C.: Parts-per-billion mass measurement accuracy achieved through the combination of multiple linear regression and automatic gain control in a fourier transform ion cyclotron resonance mass spectrometer. *Anal. Chem.* **79**, 5058–5063 (2007)

24. Kang, H., Paša-Tolić, L., Smith, R.D.: Targeted tandem mass spectrometry for high-throughput comparative proteomics employing NanoLC-FTICR MS with external ion dissociation. *J. Am. Soc. Mass Spectrom.* **18**, 1332–1343 (2007)

25. Senko, M.W., Hendrickson, C.L., Emmett, M.R., Shi, S.D.H., Marshall, A.G.: External accumulation of ions for enhanced electrospray ionization fourier transform ion cyclotron resonance mass spectrometry. *J. Am. Soc. Mass Spectrom.* **8**, 970–976 (1997)